



**HAL**  
open science

## Systematic $H_2 / H_\infty$ haptic shared control synthesis for cars, parameterized by sharing level

Béatrice Pano, Fabien Claveau, Philippe Chevrel, Chouki Sentouh, Franck Mars

► **To cite this version:**

Béatrice Pano, Fabien Claveau, Philippe Chevrel, Chouki Sentouh, Franck Mars. Systematic  $H_2 / H_\infty$  haptic shared control synthesis for cars, parameterized by sharing level. SMC 2020: IEEE International Conference on Systems, Man, and Cybernetics, Oct 2020, Toronto, Canada. 10.1109/SMC42975.2020.9283441 . hal-02929610

**HAL Id: hal-02929610**

**<https://hal.science/hal-02929610v1>**

Submitted on 3 Sep 2020

**HAL** is a multi-disciplinary open access archive for the deposit and dissemination of scientific research documents, whether they are published or not. The documents may come from teaching and research institutions in France or abroad, or from public or private research centers.

L'archive ouverte pluridisciplinaire **HAL**, est destinée au dépôt et à la diffusion de documents scientifiques de niveau recherche, publiés ou non, émanant des établissements d'enseignement et de recherche français ou étrangers, des laboratoires publics ou privés.

# Systematic $H_2/H_\infty$ haptic shared control synthesis for cars, parameterized by sharing level

Béatrice Pano<sup>1</sup>, Fabien Claveau<sup>1</sup>, Philippe Chevrel<sup>1</sup>, Chouki Sentouh<sup>2</sup>, Franck Mars<sup>3</sup>

**Abstract**—This paper presents a methodology for the systematic synthesis of haptic shared control (HSC) of a car. This HSC design is based on a two-part architecture. The first part is a trajectory generator that provides a reference trajectory to the second part, which is a static output feedback. In this paper, the haptic shared control is used as an lane keeping assist system (LKA); hence, the reference trajectory is chosen to fulfill this function. The main contribution of this article is related to the combination of the  $H_2/H_\infty$  feedback synthesis. This, involves an  $H_2$  criterion quantifying the sharing level and quality as an objective function, and  $H_2/H_\infty$  constraints for lane-keeping performance, driver comfort and robustness. The control design relies on a driver cybernetic model, which decreases conflicts between the assistance and the driver. A systematic method to tune criterion and constraints is described, enabling the attainment of desired lane-following and shared-control performance. The proposed methodology facilitates the design of lateral assistance, ensuring stability and guaranteed performance regardless of the prescribed level of sharing between the actions of the driver and the automaton. The shared control between human driver and automation for the lane keeping task over the Satory test track with the sharing level adaptation is then shown for the validation of the proposed architecture. This work introduces perspectives on smooth transitioning between manual and autonomous driving modes.

## I. INTRODUCTION

Autonomous vehicles are considered to be a possible solution for reducing the number of car accidents that occur each year. Indeed, human error is the most common accident cause [1]. But this technology must still be adapted to all driving situations. Autonomous vehicles cannot deal with some complex situations, such as road-works or unexpected circumstances. Hence, it is important to investigate intermediate solutions like haptic shared control (HSC) for lane-keeping assistance (LKA). In addition, research has shown that HSC gives better results than either human or autonomous driving alone, in cases of human or autonomous-system errors in a context of obstacle avoidance [2]. HSC systems allow the human and the machine to exchange information through the steering wheel as a haptic interface. They can then act together, with the benefit of both the driver judgement capacity and the rapidity of the machine.

<sup>1</sup>Laboratoire des Sciences du Numérique de Nantes (LS2N UMR CNRS 6004), IMT-Atlantique, 44307 Nantes, France, e-mails : first-name.lastname@ls2n.fr

<sup>2</sup>Laboratoire d'Automatique, de Mécanique et d'Informatique industrielles et Humaines (LAMIH UMR CNRS 8201), Université Polytechnique Hauts-de-France, 59300 Valenciennes, France, e-mail: Chouki.Sentouh@uphf.fr

<sup>3</sup>Laboratoire des Sciences du Numérique de Nantes (LS2N UMR CNRS 6004), CNRS & Centrale Nantes, 44321 Nantes, France, e-mail: Franck.Mars@ls2n.fr

Various HSC systems have been reported in the literature in recent years [3] [4] [5] [6] [7]. An important point to develop an HSC system is the need to use a driver model [8]. The driver model gives the system information about drivers behavior and allows to reduce the conflicts between the machine and the driver.

The use of HSC systems can also help to develop smooth transitional strategies between manual and autonomous driving modes [9]. Some researchers have investigated this possibility with different HSC systems [10] [11]. To use an HSC system to perform transition between manual and autonomous driving, it is advisable to employ the same architecture for manual, autonomous and shared-driving modes [12]. This ensures continuity in the assistance behavior, which is important because unexpected action from the assistance can be dangerous. It can also decrease the driver acceptance.

The aim of this article is to develop an HSC system design methodology that can be used at any level of sharing between the manual and autonomous modes. The main contribution of this article is a comprehensive design methodology for an advanced HSC system. This methodology facilitates the synthesis of lateral assistance, ensuring stability and a guaranteed level of performance, regardless of the degree of sharing in the actions of the driver and the automaton. The general architecture of the HSC system is inspired from previous research [7]. There are two parts: an anticipatory part that provides a reference trajectory to the compensatory part, which is static output feedback.

In this paper, the feedforward part remains the same. The original results presented here focus on the design of the feedback part and the systematic calibration methodology used to tune it. Recently, many HSC systems were developed using model predictive control (MPC) [13] [14], fuzzy control [5] [15] or  $H_2$  and  $H_\infty$  optimal controllers [3] [16] [17], for example. Here, we have used an optimal controller with several  $H_2$  and  $H_\infty$  objectives. Drawing on the strengths of a cybernetic driver model [7], [18], the proposed design methodology is based on an  $H_2$  criterion that can easily be tuned to provide the desired sharing level. Several  $H_2$  or  $H_\infty$  constraints are considered to allow for the compromises between trajectory-tracking performance, passenger comfort, and robustness.

This paper is organized in five sections. After the introduction, section II describes the driver and car models used to design the HSC system and to provide simulations for the results section. Then, section III introduces the main contribution of this article, that is, the HSC system design methodology; this

TABLE I  
DRIVER MODEL PARAMETERS

$K_p$	Anticipation gain	3.4
$K_c$	Compensation gain	15
$T_I$	Compensation frequency band	1
$T_L$	Compensation rate	3
$\tau_p$	Human processing time delay	0.04
$K_r$	Steering column stiffness	1
$K_t$	Steering-wheel holding stiffness	12
$T_N$	Neuromuscular time constant	0.1

section also discusses the systematic tuning of the  $H_2/H_\infty$  criterion and constraints. Section IV describes simulations performed to validate the HSC system and discusses the results obtained. Finally, a conclusion is presented in the last section.

## II. MODEL DESCRIPTION

Two different models are used in this paper: a driver model and a vehicle-road model. The first, previously developed in [18] [19], is used for both the simulation of the driver-in-the-loop system and also for the integration of driver's behaviors into the control design procedure, and consists of a cybernetic model of the driver. This model accounts for each step of the driving task, from visual perception to the driver's arm turning the steering wheel (see Figure 1 and parameter definitions in Table I). Inputs of the driver model are, first, the angle to the near point,  $\theta_{near}$ , situated at a distance  $l_s$  from the front of the vehicle; and second, the angle to the far point,  $\theta_{far}$ , situated at the tangent point between the edge of the lane and the driver sight. The output of this driver model is the torque applied on the steering wheel,  $\Gamma_d$ . The  $\Gamma_s$  term is the self-aligning torque;  $\delta_d$  is the steering-wheel angle. The driver model does not depend on the HSC system, it was identified while in manual mode. Equations of the driver model are provided in [7]. The vehicle-

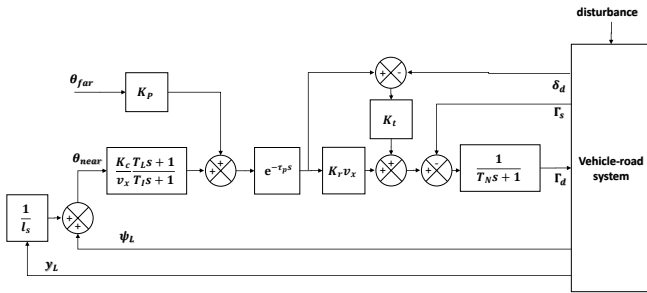


Fig. 1. Driver model diagram according to [18]

road model includes a linear bicycle model to represent the vehicle lateral dynamics, a model of the positioning dynamics of the vehicle on the road and a steering-column model. This model is parametrized using a fixed longitudinal speed,  $v_x$ . The steering-column model architecture is specified in Figure 3 and vehicle-road parameter values are defined in Table II. Based

TABLE II  
VEHICLE-ROAD MODEL PARAMETERS VALUES

$l_f$	Distance from gravity center to front axle	1.289 m
$l_r$	Distance from gravity center to rear axle	1.611 m
$m$	Total mass of the vehicle	1834.9 kg
$J$	Vehicle yaw moment of inertia	2800 kg.m <sup>2</sup>
$C_{f0}$	Front cornering stiffness	64807 N/rad
$C_{r0}$	Rear cornering stiffness	68263 N/rad
$\eta_t$	Tire length contact	0.245 m
$\nu$	Adhesion	0.8
$K_m$	Manual steering column gain	0.031
$R_s$	Steering-gear ratio	14.54
$B_s$	Steering-system damping coefficient	1.0173
$I_s$	Inertial moment of steering system	0.0891 kg.m <sup>2</sup>
$\mu_s$	Spring stiffness	0.9141 N.m/rad
$l_s$	Look-ahead distance	5m
$v_x$	Longitudinal speed	18m/s
$D_{far}$	Distance to the tangent point	15 m

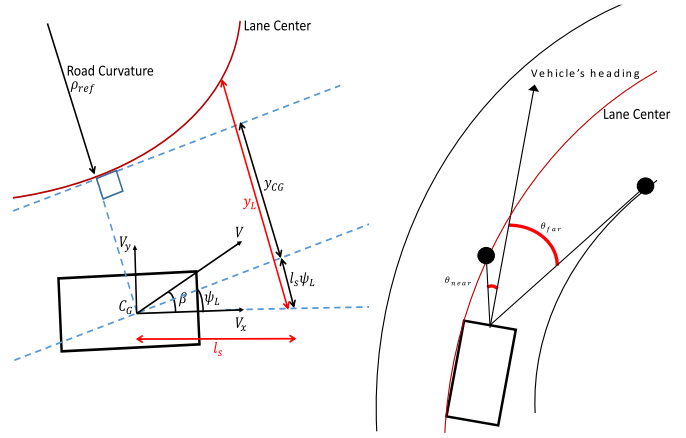


Fig. 2. Vehicle position on the road compared to the lane center

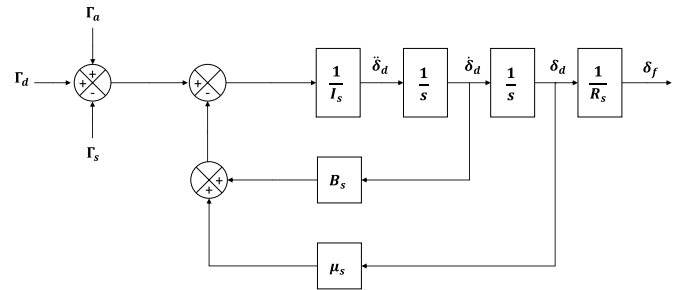


Fig. 3. Steering-column model diagram

on previous results [3], a state-space model of the vehicle-road system was obtained, as follows:

$$\dot{x}_{vr} = A_{vr} x_{vr} + B1_{vr} (\Gamma_a + \Gamma_d) + B2_{vr} \begin{bmatrix} F_w \\ \rho_{ref} \end{bmatrix} \quad (1)$$

where  $x_{vr} = [\beta \ r \ \psi_L \ y_L \ \delta_d \ \dot{\delta}_d]^T$ ;  $\beta$  is the side slip angle;  $r$  is the yaw rate;  $\psi_L$  is the heading error;  $y_L$  is the lateral deviation;  $\delta_d$  is the steering-wheel angle;  $\Gamma_a$  is the assistance torque calculated by the HSC system;  $F_w$  is the lateral wind force resultant and  $\rho_{ref}$  is the road curvature, calculated at a

distance  $l_s$  in front of the vehicle. Some of these values are illustrated in Figure 2. In Figure 3,  $\delta_f$  is the wheel angle.

$$A_{vr} = \begin{bmatrix} a_{11} & a_{12} & 0 & 0 & \frac{b_1}{R_s} & 0 \\ a_{21} & a_{22} & 0 & 0 & \frac{b_2}{R_s} & 0 \\ 0 & 1 & 0 & 0 & 0 & 0 \\ v_x & l_s & v_x & 0 & 0 & 0 \\ 0 & 0 & 0 & 0 & 0 & 1 \\ \frac{T_{s\beta}}{I_s} & \frac{T_{sr}}{I_s} & 0 & 0 & -\frac{T_{s\beta}}{R_s I_s} - \frac{\mu_s}{I_s} & -\frac{B_s}{I_s} \end{bmatrix} \quad (2)$$

$$B1_{vr} = \begin{bmatrix} 0 \\ 0 \\ 0 \\ 0 \\ 0 \\ \frac{1}{I_s} \end{bmatrix}, B2_{vr} = \begin{bmatrix} e_{11} & 0 \\ e_{22} & 0 \\ 0 & -v_x \\ 0 & -l_s v_x \\ 0 & 0 \\ 0 & 0 \end{bmatrix} \quad (3)$$

Expressions for parameters  $a_{11}$ ,  $a_{12}$ ,  $a_{21}$ ,  $a_{22}$ ,  $b_1$ ,  $b_2$ ,  $T_{s\beta}$ ,  $T_{sr}$ ,  $e_{11}$  and  $e_{22}$  are given in [3]. The vehicle-road model parameters listed in Table II were calculated by identifying a vehicle model used on a driving simulator SCANeR-AVSimulation [20].

### III. HAPTIC SHARED CONTROL STRATEGY

#### A. Global architecture

The HSC system developed in this article is aimed at assisting the driver in the steering task. Specifically, the aim is to provide part of the steering torque while avoiding conflicts with the driver when possible. The global architecture chosen for this HSC system was designed in [7] and is illustrated in that work. It is shown in Figure 4 of this paper.

To fulfill the steering task, the HSC system has two complementary parts: a reference trajectory generator with an anticipatory action and a static output feedback with a compensatory action. The reference trajectory generator is the same as in [7]. It provides a reference trajectory composed of a reference torque,  $\Gamma_{ref}$ , and a reference vehicle-road state,  $x_{ref}$ , which depends on the road curvature. The reference trajectory is found by simulating a virtual vehicle driving on the same road as the real vehicle. The virtual vehicle is an autonomous vehicle steered by an  $H_2/preview$  system. The autonomous vehicle has precise lane-following so that the virtual vehicle stays close to the lane center but it does not consider driver preferences.

The static output feedback is synthesized using an  $H_2/H_\infty$  approach. The feedback synthesis should consider various aspects: lane-following performance, driver comfort, sharing performance and robustness. Lane-following performance and driver comfort are considered  $H_2$  constraints; robustness is an  $H_\infty$  constraint. These constraints must be respected during the driving. Hence, the vehicle should not deviate from the reference trajectory within a certain margin defined by lane-following constraints. These constraints are defined according to the driver model performance in a systematic way. Sharing performance is considered using an  $H_2$  criterion, depending on the input sharing level  $\alpha$ . Then, this methodology should result in an HSC system that follows the reference trajectory and

ensures driver comfort and system robustness while attaining the required sharing level to the extent possible.

Inputs of the HSC system are  $\rho_{previewed}$  and  $F_w$ . The  $\rho_{previewed}$  term is the road curvature, previewed at a distance  $v_x T_{horizon}$  ahead. The  $F_w$  term is the lateral wind force resultant.

In Figure 4, the sharing level,  $\alpha$  (which is the assistance torque compared with the total torque applied on the steering wheel), is applied in both the anticipatory and compensatory parts. Concerning the reference trajectory generator, it is applied as  $\Gamma_{a,ff} = \alpha \Gamma_{ref}$ . For the static output feedback, it appears in the criterion used to design the feedback law.

#### B. Feedback synthesis

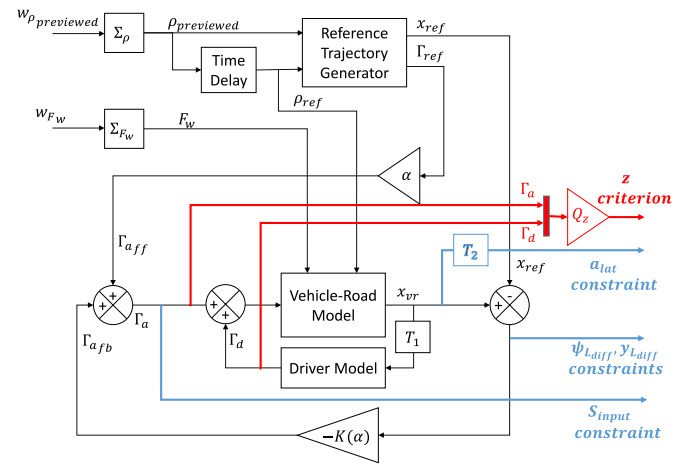


Fig. 4. Global haptic shared control, showing criterion and constraints used to synthesize the static output feedback

Figure 4 is a diagram of the global haptic shared control. Here, the  $T_1$  block represents calculations performed on  $x_{vr}$  to obtain driver model inputs. The  $T_2$  block yields the lateral acceleration  $a_{lat}$ . The feedback law can be defined as follows:

$$\Gamma_{a,fb} = -K(\alpha)(x_{vr} - x_{ref}) \quad (4)$$

where  $K(\alpha)$  is a static gain, which implicitly depends on the sharing level ( $\alpha$ ) defined in the standard model (see Figure 4); and  $x_{ref} = [\beta_{ref} \ r_{ref} \ \psi_{Lref} \ y_{Lref} \ \delta_{dref} \ \dot{\delta}_{dref}]^T$  is the virtual vehicle state.

To specify the dynamic of the exogenous inputs  $\rho_{previewed}$  and  $F_w$ , a generator model is used for each input, respectively called  $\Sigma_\rho$  and  $\Sigma_{F_w}$ . The  $w_{\rho_{previewed}}$  and  $w_{F_w}$  terms are input signals of these models; they are considered to be unpredictable signals. These models have the same structure as the work proposed in [21]. Their impulse responses are shown in Figure 5 and they are defined as follows:

$$\Sigma_\rho = \frac{K_\rho}{(1 + \tau_\rho s)(\omega_\rho^2 s^2 + \frac{2\xi_\rho}{\omega_\rho} s + 1)} \quad (5)$$

$$\Sigma_{F_w} = \frac{K_w}{(\omega_w^2 s^2 + \frac{2\xi_w}{\omega_w} s + 1)} \quad (6)$$

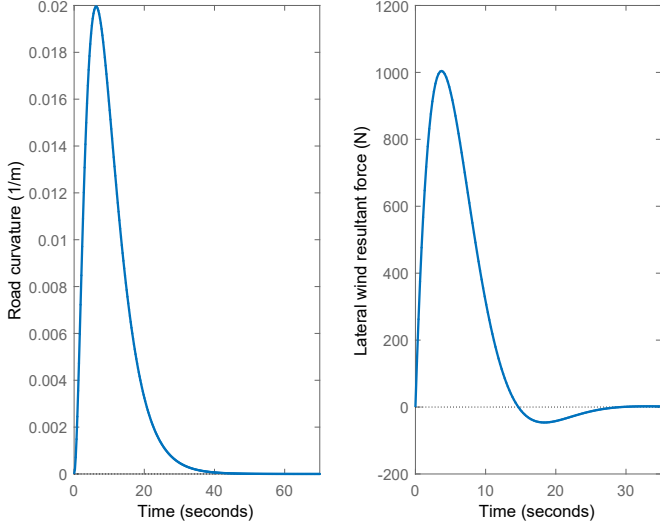


Fig. 5. Impulse responses of generator models for road curvature and lateral wind-force resultant

The control problem consists of an  $H_2$  criterion to minimize under  $H_2$  and  $H_\infty$  constraints. The  $H_2$  criterion vector allows for controlling the sharing level and avoiding conflicts between the driver and the assistance. It can be written as:

$$z = Q_z [\Gamma_d \quad \Gamma_a]^T \quad (7)$$

With :

$$Q_z = \begin{bmatrix} c_d & c_{da} \\ 0 & c_a \end{bmatrix} \quad (8)$$

The  $H_2$  constraints are defined to improve driver comfort through lateral acceleration,  $a_{lat}$ , and lane-following performance. Here, the real lateral deviation is compared to the reference deviation,  $y_{L_{diff}} = y_L - y_{L_{ref}}$ , and the real heading error is compared to the reference error,  $\psi_{L_{diff}} = \psi_L - \psi_{L_{ref}}$ . Two  $H_2$  norms are constrained for each value, according to the road curvature and according to the lateral wind force. The reference trajectory can be different from the lane center such as in the case of a lane change. An  $H_\infty$  constraint is added to the input sensitivity of the whole closed-loop system to ensure its robustness.

Finally, the control problem is defined as follows:

$$P : \left\{ \begin{array}{l} \text{Find } K \text{ such that:} \\ \min_K (\|T_{(w_\rho, w_{F_w}) \rightarrow z}\|_2) \\ \text{under constraints:} \\ \|T_{w_\rho \rightarrow \psi_{L_{diff}}}\|_2 \leq c_{\rho \rightarrow \psi_{L_{diff}}} \\ \|T_{w_\rho \rightarrow y_{L_{diff}}}\|_2 \leq c_{\rho \rightarrow y_{L_{diff}}} \\ \|T_{w_\rho \rightarrow a_{lat}}\|_2 \leq c_{\rho \rightarrow a_{lat}} \\ \|T_{w_{F_w} \rightarrow \psi_{L_{diff}}}\|_2 \leq c_{F_w \rightarrow \psi_{L_{diff}}} \\ \|T_{w_{F_w} \rightarrow y_{L_{diff}}}\|_2 \leq c_{F_w \rightarrow y_{L_{diff}}} \\ \|T_{w_{F_w} \rightarrow a_{lat}}\|_2 \leq c_{F_w \rightarrow a_{lat}} \\ \|S_{input}\|_\infty \leq S_{max} \end{array} \right. \quad (9)$$

To solve this non-convex control problem, the optimization tool Systune on Matlab was used. Finally, the control problem to be solved involves a criterion and several constraints with practical physical meaning. Separating the different constraints according to the exogenous inputs  $\rho_{previewed}$  or  $F_w$  enables more accurate tuning. However, initially the multiplication of the tuning parameters can be seen as a disadvantage. Hence, a systematic methodology is proposed here to compensate for this drawback.

### 1) Parametrized $H_2$ control strategy under constraints:

Before discussing the control strategy, here are some key definitions. The norm of  $x$  and the scalar product of  $x$  and  $y$ , two signals in  $L_2(\mathbb{R})$ , can be defined as follows:

$$\|x\|_2 = \sqrt{\int_{-\infty}^{+\infty} x^2(t) dt} \quad (10)$$

$$\langle x|y \rangle = \int_{-\infty}^{+\infty} x^T(t)y(t) dt = \|x\|_2 \|y\|_2 \cos \phi \quad (11)$$

where  $\phi = \text{angle}(x, y)$ .

To tune the criterion, the matrix  $Q_z$  must be calculated according to the sharing level ( $\alpha$ ). The instantaneous level of sharing is defined as:

$$\alpha = \frac{\Gamma_a}{\Gamma_a + \Gamma_d} \quad (12)$$

Then, to respect the sharing level, the equation  $\Gamma_a - \alpha(\Gamma_a + \Gamma_d) = 0$  is obtained in the ideal case. By squaring and integrating this equation, the expression becomes:

$$(1 - \alpha)^2 \|\Gamma_a\|_2^2 - 2\alpha(1 - \alpha) \langle \Gamma_d | \Gamma_a \rangle + \alpha^2 \|\Gamma_d\|_2^2 = 0 \quad (13)$$

Moreover, the  $H_2$  norm of  $z$  is given by:

$$\|z\|_2^2 = (c_a^2 + c_{da}^2) \|\Gamma_a\|_2^2 + 2c_d c_{da} \langle \Gamma_d | \Gamma_a \rangle + c_d^2 \|\Gamma_d\|_2^2 \quad (14)$$

Then, comparing equations (13) and (14), the parameters of  $Q_z$  are found through  $c_d = \alpha$ ,  $c_a = 0$  and  $c_{da} = (\alpha - 1)$ .

This criterion is easy to tune for any sharing level from 0 (manual mode) to 1 (autonomous mode). It also minimizes any conflicts between the driver and the assistance; the reason is that a positive scalar product between  $\Gamma_a$  and  $\Gamma_d$  results in a decreased value of  $\|z\|_2$ .

2) *Systematic choice of constraint bounds:* To ensure lane-following performance and driver comfort, the six first constraint bounds in (9) must be compatible with the objectives. A trade-off is necessary between performance and driver acceptability. For example, if the trajectory generator is tuned to keep the vehicle as close as possible to the lane center, conflicts can occur with a driver who does not always stay at the lane center, especially during curves. More generally, according to [22], this conflict can arise through too much or too little assistance torque or an assistance action that occurs too early or too late. Concretely, constraint parameters are calculated using the  $H_2$  norms computed from the  $\|T_{w_i \rightarrow y_i}\|_2$  transfers. This considers the global augmented system, namely the driver-vehicle-road model plus the exogenous signal model (see Figure 6), so

it includes the driver model but without feedback assistance. Equation (15) shows the constraint calculation where  $u_i$  is  $\rho_{previewed}$  or  $F_w$ , the  $y_i$  term is  $\psi_{L_{diff}}$  or  $y_{L_{diff}}$  or  $a_{lat}$ , the  $w_i$  term is  $w_{\rho_{previewed}}$  or  $w_{F_w}$  and the value of  $p(u_i, y_i)$  is the tolerance margin considered as a percentage. Once these values are computed, a +20% margin is considered for each value to obtain the final bounds for synthesis.

$$c_{u_i \rightarrow y_i} = (1 + p(u_i, y_i)) \|T_{w_i \rightarrow y_i}\|_2 \quad (15)$$

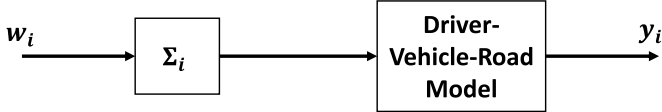


Fig. 6. Model used to calculate constraint bounds using the value of the  $H_2$  norm  $\|T_{w_i \rightarrow y_i}\|_2$

#### IV. SIMULATION TESTS

##### A. Simulator description and scenarios

In this article, we propose a new HSC design methodology that can be used for every sharing level from manual to autonomous mode. To validate this methodology, we performed simulations using different levels of sharing. The experiments were carried out with a Matlab/Simulink simulator. The design models for the driver and the vehicle were used. In addition, a geometric estimator was used to estimate the position of the vehicle on the road; that is, to compute the necessary signals such that  $y_L$ ,  $\psi_L$  and inputs of the driver model ( $\theta_{near}$  and  $\theta_{far}$ ).

Two simulations were conducted for each sharing level considered. The first simulation employed the track in Figure 7 to test driver and assistance behavior while following a realistic road. The second simulation tested the effect of the wind force on the system. The wind force applied was a step function of 1000N that lasted 5 sec. These simulations were performed for five sharing levels: 0%, 20%, 50%, 80% and 100%. A last case was considered for each simulation with a sharing level  $\alpha = 100\%$  and without the driver in order to validate the assistance behavior in autonomous mode. All simulations were performed with a fixed longitudinal speed of  $v_x = 18$  m/s.

##### B. Tuning

Driver and vehicle models were tuned according to the parameter values in Tables I and II. The values employed to define  $\Sigma_\rho$  and  $\Sigma_{F_w}$  were as follows:  $K_\rho = 0.245$ ,  $\tau_\rho = 5s$ ,  $\xi_\rho = 1$ ,  $\omega_\rho = 0.4rad/s$ ,  $K_w = 7300$ ,  $\xi_w = 0.7$  and  $\omega_w = 0.3rad/s$ . The  $H_2$  criterion was tuned based on the chosen sharing level according to (13) and (14). The six first constraint parameters were computed considering a first set of 20% as tolerance margins. Finally, a tolerance margin of 50% was chosen for the constraints on  $y_{L_{diff}}$  according to the input  $\rho_{previewed}$ , while the 20% value was retained for the five other constraints. These margins were chosen heuristically, not too high to ensure good

lane following and comfort performance and not too low to reduce conflicts with the driver model. Constraint parameters calculated were thus:  $c_{\rho \rightarrow \psi_{L_{diff}}} = 0.09$ ,  $c_{\rho \rightarrow y_{L_{diff}}} = 7.42$ ,  $c_{\rho \rightarrow a_{lat}} = 0.19$ ,  $c_{F_w \rightarrow \psi_{L_{diff}}} = 0.01$ ,  $c_{F_w \rightarrow y_{L_{diff}}} = 0.68$  and  $c_{F_w \rightarrow a_{lat}} = 1.30$ . Concerning the robustness constraint,  $S_{max}$  was chosen as equal to 2.

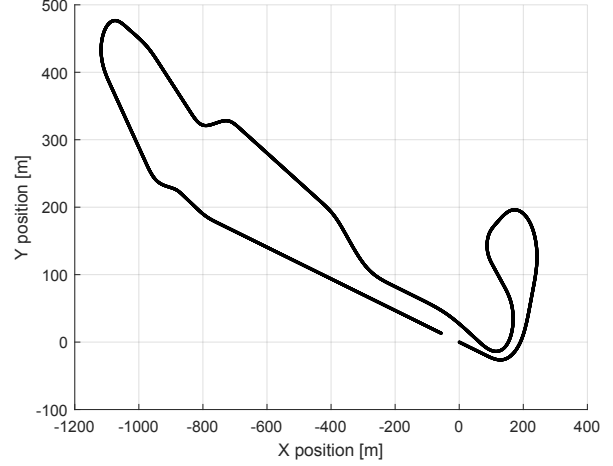


Fig. 7. Track used for simulation: track characteristics were saved for the Satory test track in Versailles

##### C. Indicators

To validate the HSC system, we needed to evaluate sharing as well as lane-following performance. The first three sharing performance indicators were the consistency ratio,  $T_{cons}$ ; the resistance ratio,  $T_{res}$  and the contradiction ratio,  $T_{cont}$ . These indicators were defined in [3].

The coherence level,  $P_c$ , is equal to the cosine between the assistance and the driver torque, expressed as:

$$P_c = \frac{\langle \Gamma_d | \Gamma_a \rangle}{\|\Gamma_a\|_2 \|\Gamma_d\|_2} \quad (16)$$

$P_c$  allows for estimating whether the assistance and the driver torques are coordinated. If  $P_c$  is equal to 1, the assistance always acts in the same direction as the driver and acts like power steering. If  $P_c$  is negative, conflicts exist between the assistance and the driver.

To estimate the sharing level that was applied during the simulation, we used the following equations:

$$\alpha_{calc} = \frac{\|\Gamma_a\|_2}{\|\Gamma_a\|_2 + \|\Gamma_d\|_2} \quad (17)$$

Lane-following performance was evaluated through the lane deviation, calculated based on the vehicle's center of gravity,  $y_{CG}$ . The driver comfort was estimated using lateral acceleration,  $a_{lat}$ .

## D. Results

1) *Simulation on a realistic track:* Results of simulations on the Satory test track are shown in Figure 8, Figure 9 and Table III. Figure 8 displays the driver and assistance torques applied on the steering wheel for each sharing level, along with the lateral deviation during simulations. Figure 9 shows two diagrams for both simulations, with  $\alpha = 50\%$  and  $\alpha = 80\%$  zoom, in one curve of the track. The first diagram shows the assistance and the driver torque applied to the steering wheel during the simulation. It also shows the driver and assistance torque that would have been applied to the steering wheel if the input sharing level was respected precisely. The second diagram shows the different parts of the assistance torque, namely the feedforward and feedback parts. Finally, Table III lists values of the various indicators during these simulations.

First, regarding lane-following performance during the simulation on a realistic track, as evident from Table III, the  $y_{CG}$  average value remained low for each sharing level (under 0.38 m). Its maximum value decreased as  $\alpha$  increased. Average and maximum values of  $y_{CG}$  were small in the autonomous mode. Moreover, Figure 8 shows that the global shape of the lateral deviation curve was mostly the same for all sharing levels except autonomous mode, in which the lateral deviation remained close to 0. These results illustrate that although the lane following algorithm is very accurate, the HSC strategy allows the driver to choose the trajectory he wants, deviating from the lane center, while reducing the effort required to achieve this trajectory.

Second, in Table III, it can be observed that the calculated sharing level,  $\alpha_{calc}$ , was almost equal to the desired sharing level before  $\alpha = 50\%$ . After this threshold,  $\alpha_{calc}$  was lower than the requested sharing level. This result is clarified in Figure 9, which focuses on one bend. Figure 9 shows that when the desired sharing level was respected ( $\alpha = 50\%$ ), the driver and assistance torque were equal to their expected values that is, 50% of the total torque. In the case of an input of  $\alpha = 80\%$ , the output is only  $\alpha_{calc} = 69\%$ . From Figure 9, it can be seen that the driver provides more than the expected 20% of the total torque if  $\alpha = \alpha_{calc}$ . The bottom right figure shows that the feedforward part of the controller alone provides almost the 80% expected torque, but the total assistance torque is ultimately reduced because of the feedback contribution.

Furthermore, until  $\alpha = 50\%$ , sharing performance was high, with a consistency ratio superior or equal to 0.80 and  $P_c$  values close to 1. This means that the assistance acted in accordance with the driver. For  $\alpha = 80\%$  and  $\alpha = 100\%$ , sharing indicator values still showed that the driver and the assistance were acting in agreement, as the  $P_c$  value was positive. However, the resistance ratio,  $T_{res}$ , increased compared to the case with lower  $\alpha$ . However, Figure 8 and Figure 9 together indicate that driver and assistance torque generally possessed the same sign during curves. Hence, it can be hypothesized that the assistance and the driver torque had different signs for small torque values.

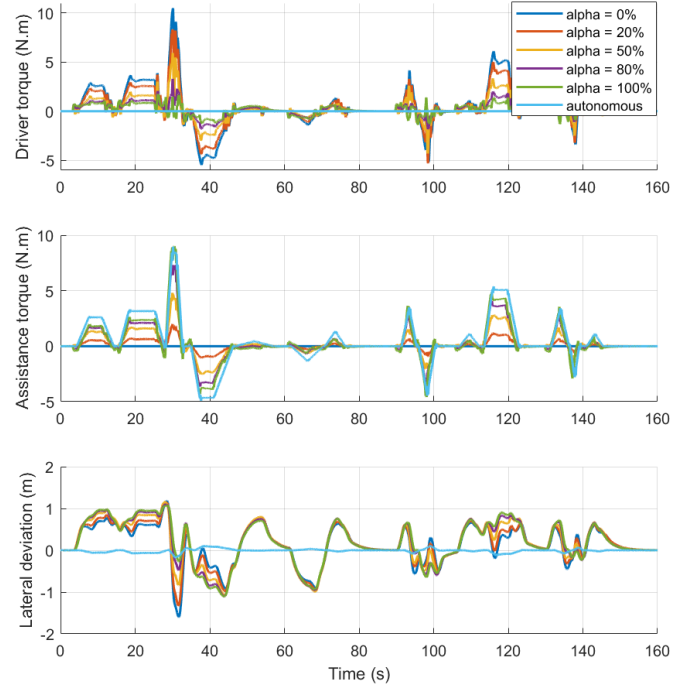


Fig. 8. Driver and assistance torque and lateral error along the track, for different levels of sharing

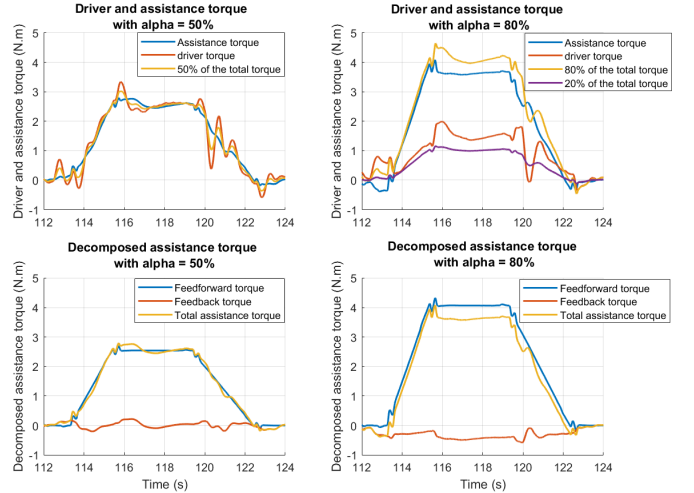


Fig. 9. Driver and assistance torque and lateral error along the track, for different levels of sharing. Zoom on a specific part of the track

2) *Effect of wind force:* Figure 10 displays driver and assistance torques for each sharing level and for autonomous mode when applying a wind force and following a straight lane. The figure also shows the lateral deviation for each simulation.

It is evident that the sharing level was respected, with driver action decreasing and assistance action rising, when  $\alpha$  increased. The assistance and the driver-torque curves are superimposed on each other for  $\alpha = 50\%$ . Moreover, the lateral deviation remained low, with a maximum value of 0.28 m for  $\alpha = 0\%$ . Lane following was increasingly precise as the sharing

TABLE III  
INDICATOR VALUES DURING SIMULATIONS

	0	20	50	80	100	auto
$max(y_{CG})(m)$	1.60	1.33	1.16	1.10	1.10	0.17
$mean(y_{CG})(m)$	0.32	0.33	0.37	0.37	0.38	0.02
$max(\Gamma_d)(N.m)$	10.48	8.32	5.92	3.29	1.74	0.00
$mean(\Gamma_d)(N.m)$	1.06	0.86	0.56	0.40	0.36	0.00
$max(\Gamma_a)(N.m)$	0.00	1.99	4.80	7.32	9.01	8.97
$mean(\Gamma_a)(N.m)$	0.00	0.21	0.52	0.70	0.82	1.02
$max(a_{lat})(m/s^2)$	12.8	12.8	12.8	12.6	12.7	12.5
$T_{cons}$	1.00	0.90	0.80	0.46	0.39	/
$T_{res}$	0.00	0.03	0.07	0.43	0.47	/
$T_{cont}$	0.00	0.07	0.14	0.12	0.14	/
$P_c$	/	0.99	0.96	0.82	0.46	/
$\alpha_{calc}$	0.00	0.20	0.49	0.69	0.76	/

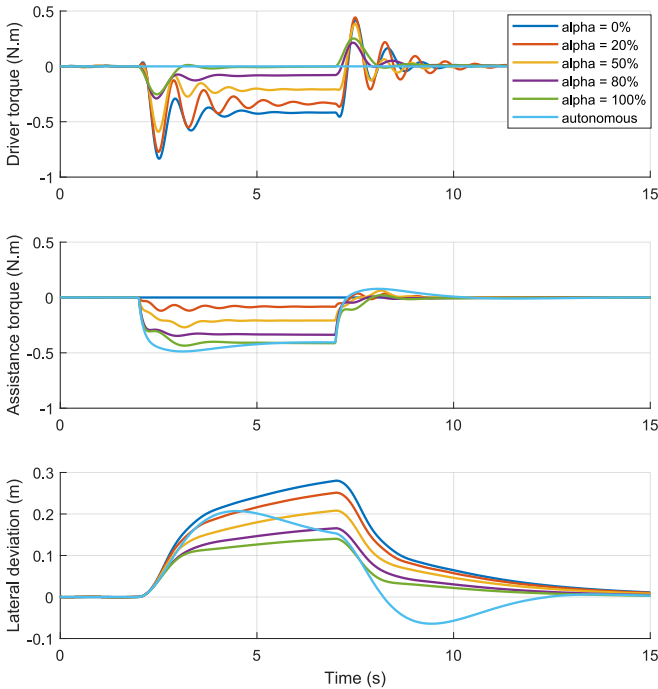


Fig. 10. Effect of wind force following a straight lane track, for different levels of sharing

level increased. It can thus be concluded that this perturbation was rejected in each case, including in autonomous mode.

### E. Discussion

The HSC methodology resulted in precise lane-following performance for both lane following and perturbation rejection. Moreover, the assistance and the driver acted in accordance most of the time.

The HSC system designed in this article allowed for precise selection of the assistance behavior. Indeed, the sharing level could be chosen easily using the criterion. In addition, the separation of constraints for lane-following performance and wind-force perturbation rejection ensured that these two aspects were given the same importance.

This system offers assistance for any sharing level from 0% to 100% with a manual and an autonomous mode. That is to say,

when  $\alpha = 0\%$ , the assistance is completely inactive; whereas  $\alpha = 100\%$  means that the assistance is able to drive alone, resulting in high performance in lane following. Therefore, this HSC system is a good candidate to develop a smooth transition method between the manual and autonomous modes.

## V. CONCLUSION

HSC systems must manage trade-offs between lane-following performance and driver acceptance. In this paper, a two-part lateral control assistance was developed toward that goal. The first part relies on a reference-trajectory generator based on the simulation of a virtual autonomous vehicle. The second part consists of an output feedback, which compensates for unforeseen behavior of the car due to model uncertainties and disturbances. Its synthesis relies on a specific  $H_2$  criterion to be minimized under various  $H_2$  and  $H_\infty$  constraints. The  $H_2$  criterion is related to the desired sharing level and the cooperation quality with the driver. The  $H_2$  and  $H_\infty$  constraints account for lane-keeping performance, driver comfort and robustness.

Simulation results showed the relevance of the methodology proposed, whatever the prescribed sharing level between actions of the driver and the automaton, from manual to autonomous mode. This HSC system now requires testing with real drivers on a driving simulator. Such testing would enable analyzing the drivers behavior and perception while they share the driving task with the assistance. Based on these results, our project will be to take profit of the proposed methodology to develop systems that provide smooth transitions between manual and autonomous driving modes through gradually modifying the level of sharing between the modes.

## ACKNOWLEDGMENT

This work was supported by AutoConduct research program, funded by the ANR "Agence Nationale de la Recherche" (grant ANR-16-CE22-0007-05).

## REFERENCES

- [1] S. G. Klauer, T. A. Dingus, V. L. Neale, J. Sudweeks, and D. J. Ramsey, "The Impact of Driver Inattention on Near-Crash/Crash Risk: An Analysis Using the 100-Car Naturalistic Driving Study Data," *National Highway Traffic Safety Administration*, Apr. 2006.
- [2] A. Bhardwaj, A. H. Ghasemi, Y. Zheng, H. Febbo, P. Jayakumar, T. Ersal, J. L. Stein, and R. B. Gillespie, "Whos the boss? Arbitrating control authority between a human driver and automation system," *Transportation Research Part F: Traffic Psychology and Behaviour*, vol. 68, pp. 144–160, Jan. 2020.
- [3] L. Saleh, P. Chevrel, F. Claveau, J. Lafay, and F. Mars, "Shared Steering Control Between a Driver and an Automation: Stability in the Presence of Driver Behavior Uncertainty," *IEEE Transactions on Intelligent Transportation Systems*, vol. 14, no. 2, pp. 974–983, Jun. 2013.
- [4] M. M. Van Paassen, R. Boink, D. Abbink, M. Mulder, and M. Mulder, "Four design choices for haptic shared control," May 2017, pp. 237–254.
- [5] M. A. Benloucif, A.-T. Nguyen, C. Sentouh, and J.-C. Poupieul, "A New Scheme for Haptic Shared Lateral Control in Highway Driving Using Trajectory Planning," *IFAC-PapersOnLine*, vol. 50, no. 1, pp. 13 834–13 840, Jul. 2017.
- [6] W. Scholtens, S. Barendswaard, D. Pool, R. Van Paassen, and D. Abbink, "A New Haptic Shared Controller Reducing Steering Conflicts," in *2018 IEEE International Conference on Systems, Man, and Cybernetics (SMC)*, Oct. 2018, pp. 2705–2710.



- [7] B. Pano, P. Chevrel, and F. Claveau, "Anticipatory and Compensatory e-Assistance for Haptic Shared Control of the Steering Wheel," in *2019 18th European Control Conference (ECC)*, Jun. 2019, pp. 724–731.
- [8] D. A. Abbink, T. Carlson, M. Mulder, J. C. F. d. Winter, F. Aminravan, T. L. Gibo, and E. R. Boer, "A Topology of Shared Control Systems-Finding Common Ground in Diversity," *IEEE Transactions on Human-Machine Systems*, vol. 48, no. 5, pp. 509–525, Oct. 2018.
- [9] M. Mulder, D. A. Abbink, M. M. v. Paassen, and M. Mulder, "Design of a Haptic Gas Pedal for Active Car-Following Support," *IEEE Transactions on Intelligent Transportation Systems*, vol. 12, no. 1, pp. 268–279, Mar. 2011.
- [10] J. Ludwig, A. Haas, M. Flad, and S. Hohmann, "A Comparison of Concepts for Control Transitions from Automation to Human," in *2018 IEEE International Conference on Systems, Man, and Cybernetics (SMC)*, Oct. 2018, pp. 3201–3206.
- [11] T. Wada, K. Sonoda, T. Okasaka, and T. Saito, "Authority transfer method from automated to manual driving via haptic shared control," in *2016 IEEE International Conference on Systems, Man, and Cybernetics (SMC)*, Oct. 2016, pp. 002 659–002 664.
- [12] M. Mulder, D. A. Abbink, and E. R. Boer, "Sharing Control With Haptics: Seamless Driver Support From Manual to Automatic Control," *Human Factors*, vol. 54, no. 5, pp. 786–798, Oct. 2012.
- [13] C. Guo, C. Sentouh, J.-C. Popieul, and J.-B. Hau, "Predictive shared steering control for driver override in automated driving: A simulator study," *Transportation Research Part F: Traffic Psychology and Behaviour*, Feb. 2018.
- [14] R. Luo, Y. Weng, Y. Wang, P. Jayakumar, M. Brudnak, V. Paul, V. Desraj, J. Stein, T. Ersal, and X. J. Yang, *A Workload Adaptive Haptic Shared Control Scheme for Semi-Autonomous Driving*, Mar. 2020.
- [15] Y. Tian, Y. Zhao, Y. Shi, X. Cao, and D.-L. Yu, "The indirect shared steering control under double loop structure of driver and automation," *IEEE/CAA Journal of Automatica Sinica*, pp. 1–14, 2020.
- [16] C. Sentouh, B. Soualmi, J. C. Popieul, and S. Debernard, "Cooperative Steering Assist Control System," in *2013 IEEE International Conference on Systems, Man, and Cybernetics*, Oct. 2013, pp. 941–946.
- [17] D. Tan, W. Chen, H. Wang, and Z. Gao, "Shared control for lane departure prevention based on the safe envelope of steering wheel angle," *Control Engineering Practice*, vol. 64, pp. 15–26, Jul. 2017.
- [18] L. Saleh, P. Chevrel, F. Mars, J.-F. Lafay, and F. Claveau, "Human-like cybernetic driver model for lane keeping," *IFAC Proceedings Volumes*, vol. 44, no. 1, pp. 4368–4373, Jan. 2011.
- [19] F. Mars, L. Saleh, P. Chevrel, F. Claveau, and J.-F. Lafay, "Modeling the Visual and Motor Control of Steering With an Eye to Shared-Control Automation," *Proceedings of the Human Factors and Ergonomics Society Annual Meeting*, vol. 55, no. 1, pp. 1422–1426, Sep. 2011.
- [20] "AVSimulation : Innovate. Simulate, Accelerate." [Online]. Available: <https://www.avsimulation.com/>
- [21] S. Mustaki, P. Chevrel, M. Yagoubi, and F. Fauvel, "Efficient Multi-Objective and Multi-Scenarios Control Synthesis Methodology for Designing a Car Lane Centering Assistance System," in *2018 European Control Conference (ECC)*, Jun. 2018, pp. 929–934.
- [22] M. Itoh, F. Flemisch, and D. Abbink, "A hierarchical framework to analyze shared control conflicts between human and machine," *IFAC-PapersOnLine*, vol. 49, no. 19, pp. 96–101, Jan. 2016.